



NOVEL SPACE VECTOR BASED GENERALIZED DISCONTINUOUS PWM ALGORITHM FOR INDUCTION MOTOR DRIVES

K. Sri Gowri¹, T. Brahmananda Reddy² and Ch. Sai Babu³

¹Department of Electrical and Electronics Engineering, R.G.M.C.E.T, Nandyal, A. P., India

²Department of Electrical and Electronics Engineering, G. Pulla Reddy Engineering College, Kurnool, A. P., India

³Department of Electrical Engineering, J. N. T. University, Anantapur, A. P., India

E-Mail: gowrivasu.3@gmail.com

ABSTRACT

This paper presents a novel space-vector based Generalized Discontinuous pulse width modulation (GDPWM) algorithm without angle estimation based on the concept of imaginary switching times. The conventional space vector pulse width modulation (CSVPWM) method with equal division of zero state vectors V_0 and V_7 is modified. A constant-variable μ and modulation phase angle δ ranging from 0 to 1 are used to generate infinite number of modulating waveforms. Also, the classical triangle comparison approach is replaced by space vector approach. To avoid the complex coordinate transformations, trigonometric calculations and sector identification involved in CSVPWM, the concept of imaginary switching times is utilized. The imaginary switching times proportional to the reference phase voltages are used to calculate the actual switching times for reduced complexity and memory required. The proposed PWM technique results in reduced current ripple over the CSVPWM at high modulation indices and low switching losses at all modulation indices. To validate the proposed method, simulation is carried out on V/f controlled induction motor and the no-load current waveforms at different modulation indices and frequencies are presented and %THDs is compared.

Keywords: CSVPWM, GDPWM, imaginary switching times.

INTRODUCTION

Any PWM strategy for power electronic conversion is based on the factors such as waveform quality and switching losses. In recent years several PWM methods gained importance among which CSVPWM is the most popular because of the numerous advantages [1, 2]. It is capable of producing highest available fundamental output voltage with low harmonic distortion in the output current and is suitable for digital implementation. In this method the reference voltage vector is synthesized by time averaging two active states and two zero states in every sampling period, T_s . However, CSVPWM suffers from the drawbacks like computational burden and inferior performance at high modulation indices. Moreover, as the CSVPWM is a continuous PWM (CPWM) method the switching losses of the inverter are also high. Hence to reduce the switching losses and to improve the performance in high modulation region several discontinuous PWM (DPWM) methods have been reported in [3-8, 10-12]. The triangle-comparison pulse width modulator compares high frequency carrier wave with the three reference sinusoidal voltages generating gate pulses for the switching devices. Adding a properly selected zero sequence signals, different discontinuous modulating waveforms can be generated. If the augmenting zero-sequence signal is continuous it produces CPWM scheme and if it is discontinuous it results in DPWM schemes. A carrier based generalized PWM method comprising of all DPWM methods is considered as generalized discontinuous PWM scheme (GDPWM) [4-6].

Among the two popular approaches, namely, triangle comparison (TC) and space vector (SV) approaches, SV approach is more general and offers more

degrees of freedom in dividing the duration of zero states compared to the TC approach [7-8]. Changing the ratio by which the two zero states are applied in SV approach produces the same effect as the conventional triangle comparison method in which a properly selected zero sequence signal is added to produce different modulators. However to reduce the computational burden involved in SV approach, the concept of imaginary switching times is proposed in [9-12].

The objective was to develop new space vector based GDPWM algorithm without angle and sector determination for reduced current ripples and switching losses at high modulation region.

CSVPWM ALGORITHM

With a three-phase voltage source inverter (VSI) there are eight possible switching states. The two states, from which no power gets transferred from source to load are termed as null vectors or zero states. The other six states called as active states. The active states can be represented by space vectors as given in (1) and divides the space vector plane into six equal sectors as shown in Figure-1 [6, 8, 12].

$$V_k = \frac{2}{3} V_{dc} * e^{j(k-1)\frac{\pi}{3}}, k = 1, 2, \dots, 6. \quad (1)$$

In the CSVPWM strategy, the desired reference voltage vector is generated by time averaging the two nearby active voltage states and two zero states in every sampling time T_s . For a given reference voltage V_{REF} at an angle α with reference to V_1 in first sector, the volt-time balance is maintained by applying the active state1 (V_1), active state2 (V_2) and two zero states (V_0 and V_7) together



for durations T_1 , T_2 and T_Z respectively, as given in (2) [12].

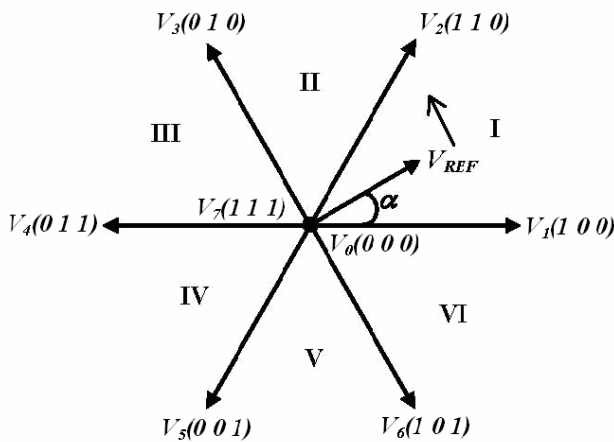


Figure-1. Switching states and corresponding voltage vectors of a three phase VSI. I, II, III, IV, V, VI are the sectors.

$$T_1 = M * \frac{\sin(60^\circ - \alpha)}{\sin 60^\circ} * T_s \quad (2.1)$$

$$T_2 = M * \frac{\sin \alpha}{\sin 60^\circ} * T_s \quad (2.2)$$

$$T_Z = T_s - T_1 - T_2 \quad (2.3)$$

Where 'M' is modulation index, given by $M = \frac{3V_{REF}}{2V_{dc}}$.

Also in CSVPWM strategy, the total zero voltage vector time, T_Z is divided equally between V_0 and V_7 . Also in this method, the zero voltage vector time is distributed symmetrically at the start and end of the sampling period in a symmetrical way. Thus, CSVPWM uses $V_0, V_k, V_{k+1}, V_7, V_{k+1}, V_k, V_0$ sequence for odd sectors and $V_0, V_{k+1}, V_k, V_7, V_k, V_{k+1}, V_0$ sequence for even sectors, respectively.

PROPOSED GDPWM ALGORITHM

As the CSVPWM is a CPWM technique, switching losses of the inverter are high. Where as in DPWM methods during each sampling period, each of the phases ceases the modulation and the associated phase is clamped to the positive dc bus or negative dc bus. Hence, the switching losses of the associated inverter leg during the period of clamping are eliminated. The performance of the PWM methods depends upon the modulation index. In the lower modulation range, the CPWM methods are superior to DPWM methods, while in the higher modulation range the DPWM methods are superior to CPWM methods. However at all the operating modulation indices, CPWM method has higher switching losses than DPWM methods. Utilizing the generalized phase shift in the DPWM methods, GDPWM algorithm is proposed in [4-6], which has more complexity due to angle calculation. Hence, to reduce the complexity involved, in this paper a

novel space vector based GDPWM method has been developed by using the concept of imaginary switching times.

The imaginary switching time periods are proportional to the instantaneous values of the phase voltages, and defined as

$$T_{as} \equiv \left(\frac{T_s}{V_{dc}} \right) V_a \quad (3.1)$$

$$T_{bs} \equiv \left(\frac{T_s}{V_{dc}} \right) V_b \quad (3.2)$$

$$T_{cs} \equiv \left(\frac{T_s}{V_{dc}} \right) V_c \quad (3.3)$$

Where T_s is the sampling period and V_{dc} is the dc link voltage. V_a , V_b and V_c are the phase voltages. Then in every sampling time, the maximum and minimum values of imaginary switching times are calculated as given in (4).

$$T_{max} = \max(T_{as}, T_{bs}, T_{cs}) \quad (4.1)$$

$$T_{min} = \min(T_{as}, T_{bs}, T_{cs}) \quad (4.2)$$

The active vector switching times T_1 and T_2 may be expressed as [12]

$$T_1 = T_{max} - T_x \quad (5.1)$$

$$T_2 = T_x - T_{min} \quad (5.2)$$

Where, $T_x \in (T_{as}, T_{bs}, T_{cs})$ and is neither maximum nor minimum switching time. The effective time is the duration in which the reference voltage vector lies in the corresponding active states, and is the difference between the maximum and minimum switching times as given by (6).

$$T_{eff} = T_1 + T_2 \quad (6)$$

The sum of zero voltage vector switching times is calculated from the sampling time and effective time as given in (7).

$$T_Z = T_s - T_{eff} \quad (7)$$

In the proposed method the zero state time will be divided between two zero states as $T_Z \mu$ for V_0 and $T_Z(1-\mu)$ for V_7 respectively, where μ lies between 0 and 1 [5, 12]. The μ can be defined as $\mu = 1 - 0.5(1 + \text{sgn}(\cos 3(\omega t + \delta)))$ where ω is the angular frequency of the reference voltage, $\text{sgn}(y)$ is the sign function, $\text{sgn}(y)$ is 1, 0, 0 and -1 when y is positive, zero and negative respectively. The modulation phase angle is represented by δ . When $\mu = 1$ any one of the phases is clamped to the positive bus for 120 degrees and when $\mu = 0$ any one of the phases is clamped to the negative bus for 120 degrees. The modulation waveforms and their zero sequence signals of few popular DPWM methods including CSVPWM method are shown in Figure-2.

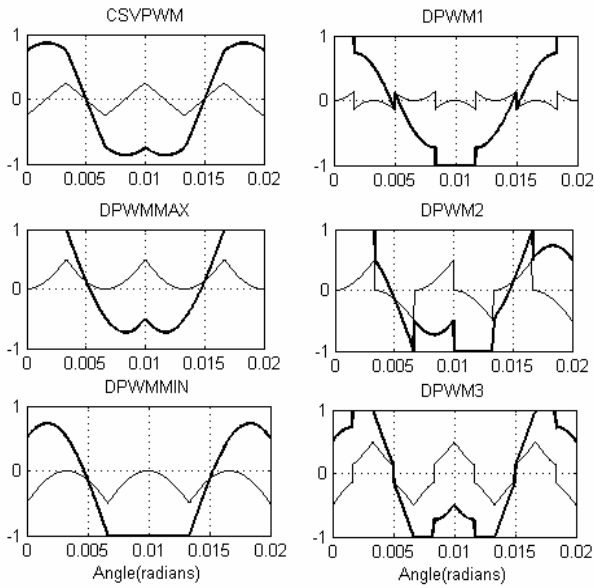


Figure-2. Modulation waveforms and their zero sequence signals of different DPWM methods.

When $\mu=0$ and $\mu=1$, DPWMMAX and DPWMMIN are obtained respectively and $\mu=0.5$ results CSVPWM. Thus, the variation of μ generates different modulating waves for different PWM methods. When $\delta=0, -\pi/6, -\pi/3$, DPWM1, DPWM2, DPWM3 can be obtained respectively [5, 12].

Thus by varying μ and δ the switching time periods of zero voltage vectors can be changed, so that different DPWM methods can be obtained.

SIMULATION RESULTS AND DISCUSSIONS

To verify the proposed algorithm, a numerical simulation has been carried out on V/f controlled induction motor drive using Matlab/Simulink at no-load for different modulation indices. The total harmonic distortion (THD) of the no-load current is used as a performance index for PWM techniques. The line current waveforms at no-load and harmonic spectra for CSVPWM and some popular DPWM methods for supply frequencies of 40Hz and 50Hz at a switching frequency of 5 KHz are shown in Figures 3 to 8. Their measured %THDs is compared (Table-1).

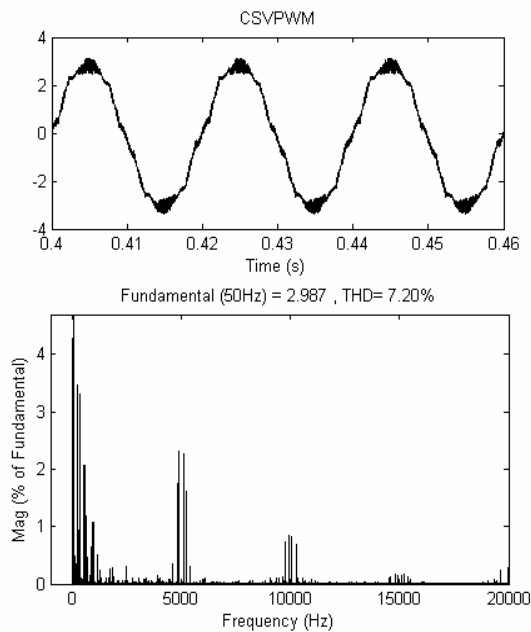


Figure-3a. Measured no-load current and harmonic spectra (% of fundamental) for CSVPWM at modulation index of 0.8.

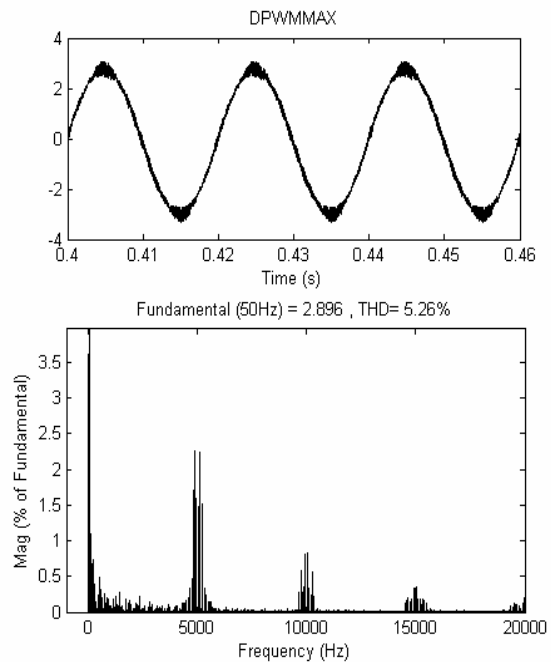


Figure-3b. Measured no-load current and harmonic spectra (% of fundamental) for DPWMMAX at modulation index of 0.8.

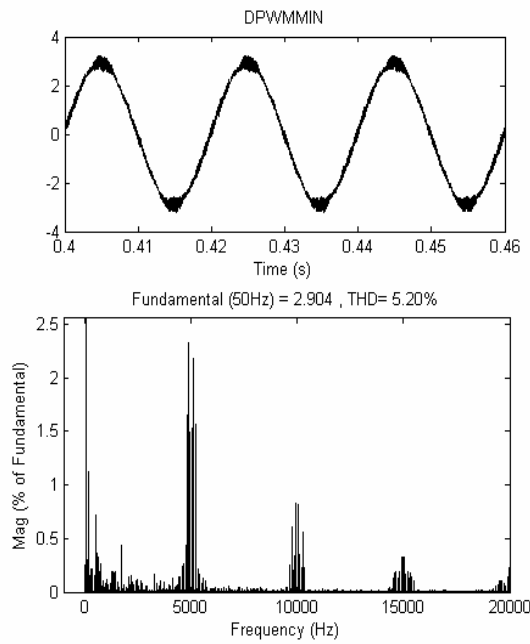


Figure-3c. Measured no-load current and harmonic spectra (% of fundamental) for DPWMMIN at modulation index of 0.8.

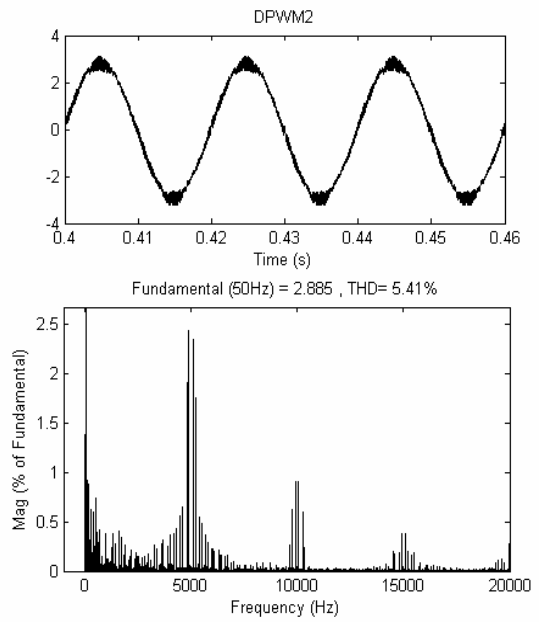


Figure-3e. Measured no-load current and harmonic spectra (% of fundamental) for DPWM2 at modulation index of 0.8.

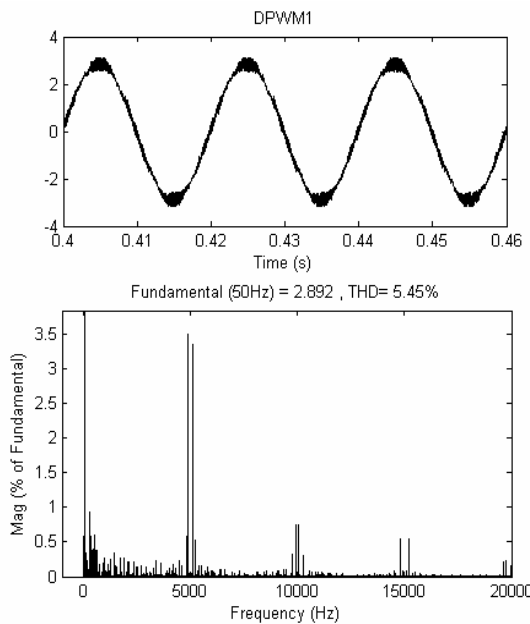


Figure-3d. Measured no-load current and harmonic spectra (% of fundamental) for DPWM1 at modulation index of 0.8.

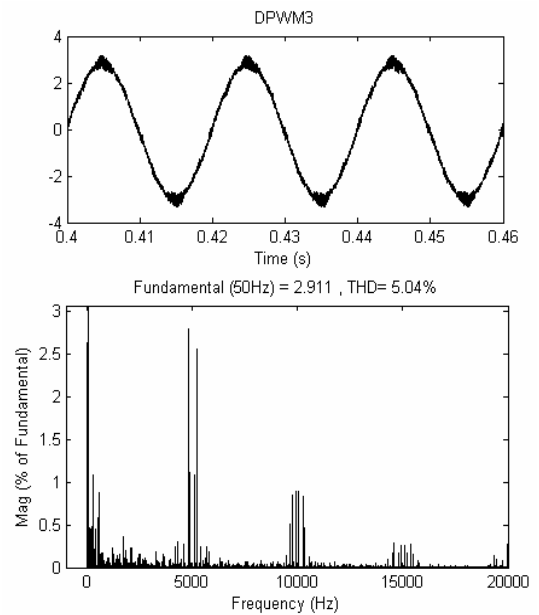


Figure-3f. Measured no-load current and harmonic spectra (% of fundamental) for DPWM3 at modulation index of 0.8.

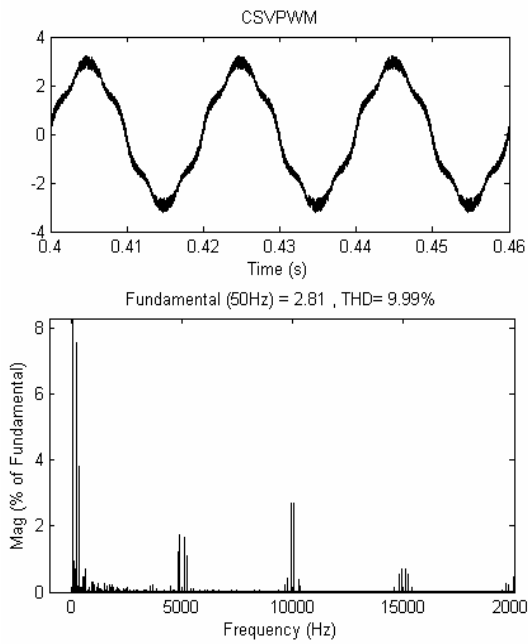


Figure-4a. Measured no-load current and harmonic spectra (% of fundamental) for CSVPWM at modulation index of 0.6.

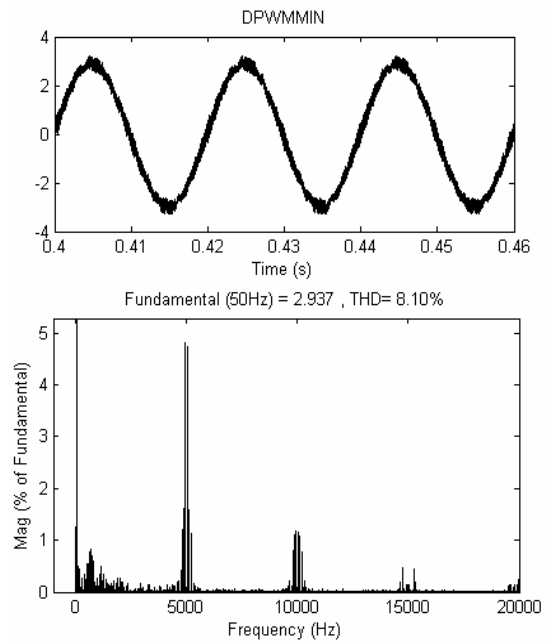


Figure-4c. Measured no-load current and harmonic spectra (% of fundamental) for DPWMI at modulation index of 0.6

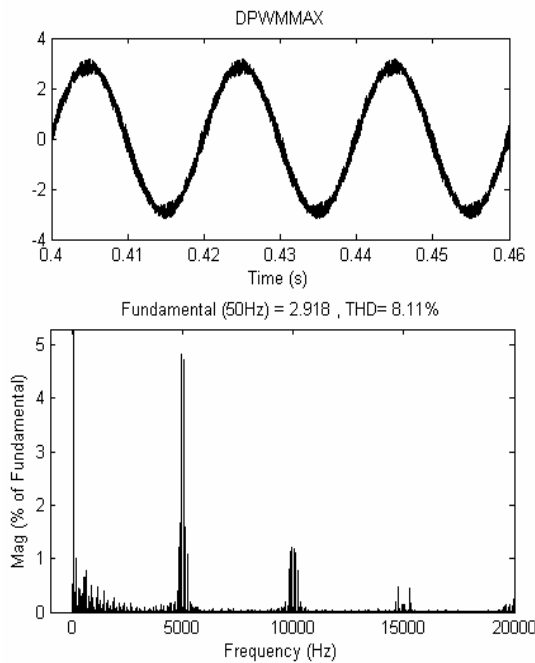


Figure-4b. Measured no-load current and harmonic spectra (% of fundamental) for DPWMMAX at modulation index of 0.6.

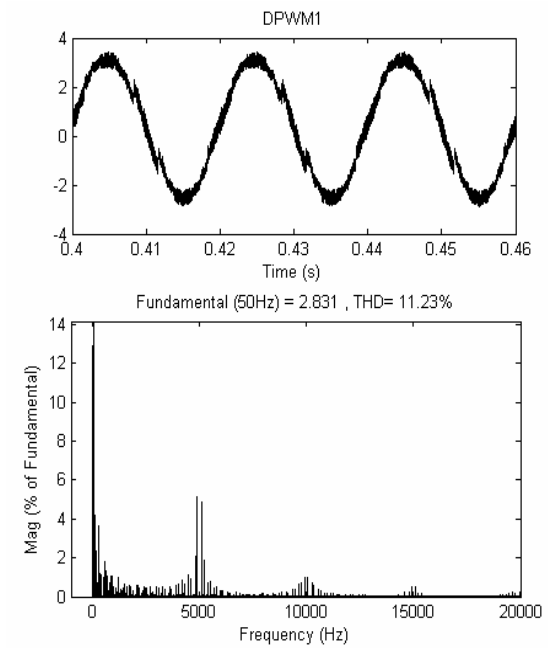


Figure-4d. Measured no-load current and harmonic spectra (% of fundamental) for DPWMI at modulation index of 0.6.

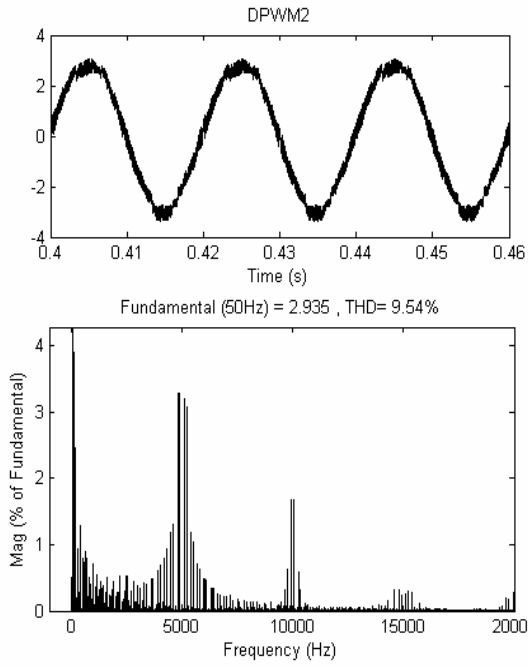


Figure-4e. Measured no-load current and harmonic spectra (% of fundamental) for DPWM2 at modulation index of 0.6.

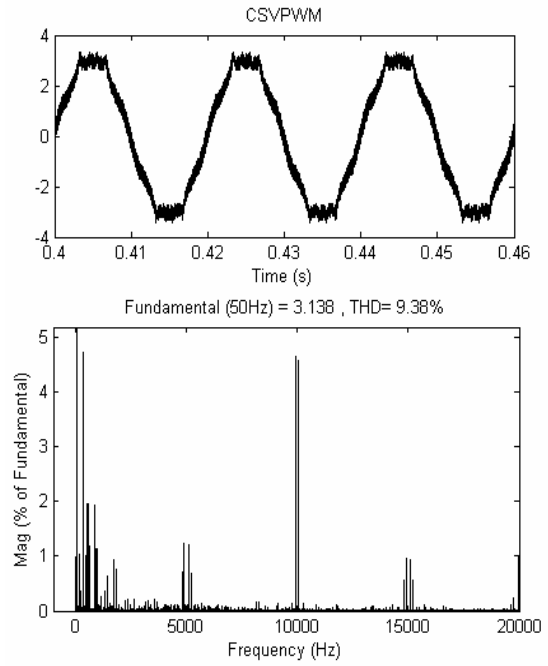


Figure-5a. Measured no-load current and harmonic spectra (% of fundamental) for CSVPWM at modulation index of 0.3.

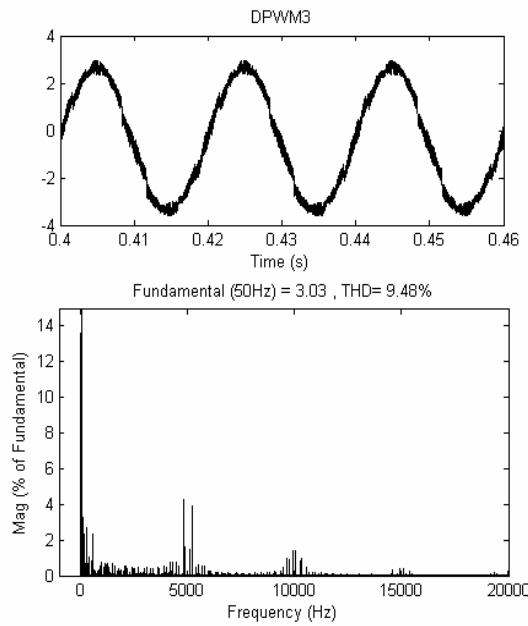


Figure-4f. Measured no-load current and harmonic spectra (% of fundamental) for DPWM3 at modulation index of 0.8.

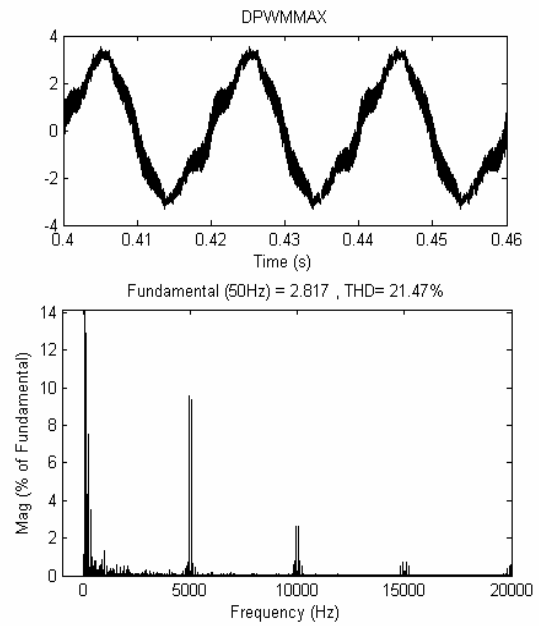


Figure-5b. Measured no-load current and harmonic spectra (% of fundamental) for DPWMMAX at modulation index of 0.3.

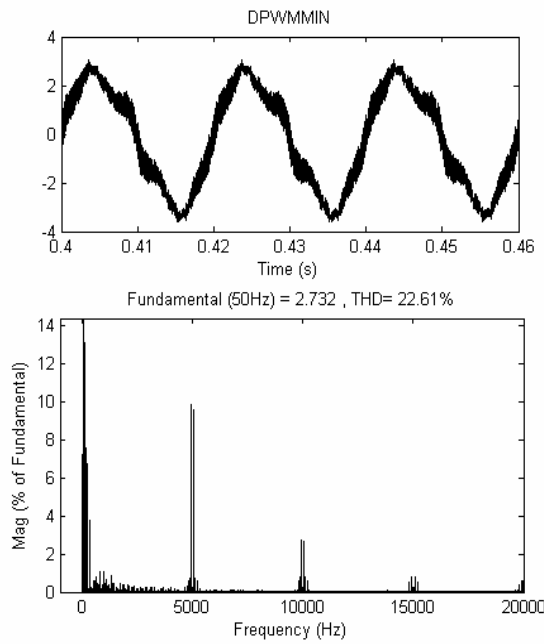


Figure-5c. Measured no-load current and harmonic spectra (% of fundamental) for DPWMMIN at modulation index of 0.3.

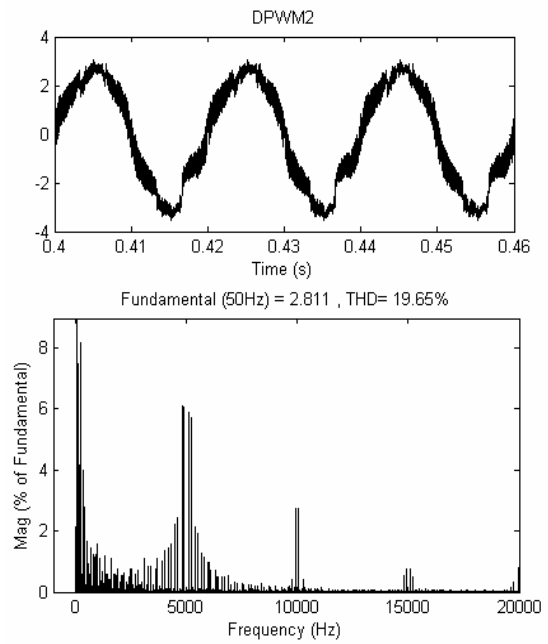


Figure-5e. Measured no-load current and harmonic spectra (% of fundamental) for DPWM2 at modulation index of 0.3.

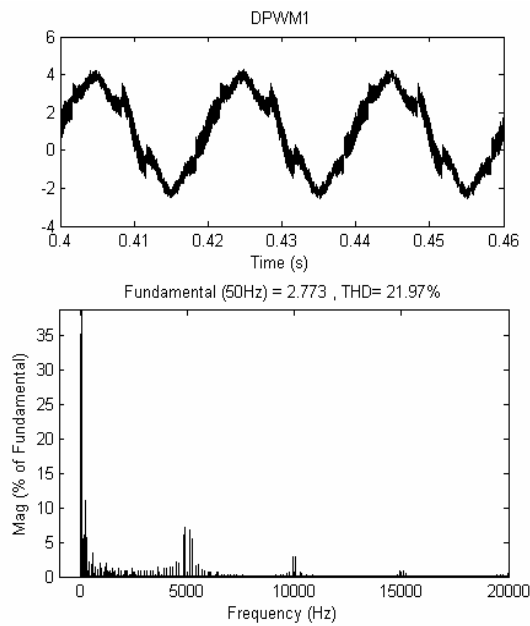


Figure-5d. Measured no-load current and harmonic spectra (% of fundamental) for DPWM1 at modulation index of 0.3.

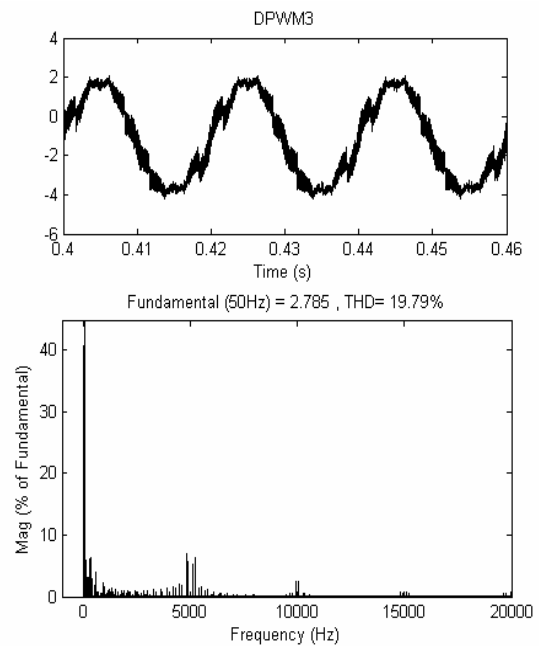


Figure-5f. Measured no-load current and harmonic spectra (% of fundamental) for DPWM3 at modulation index of 0.3.

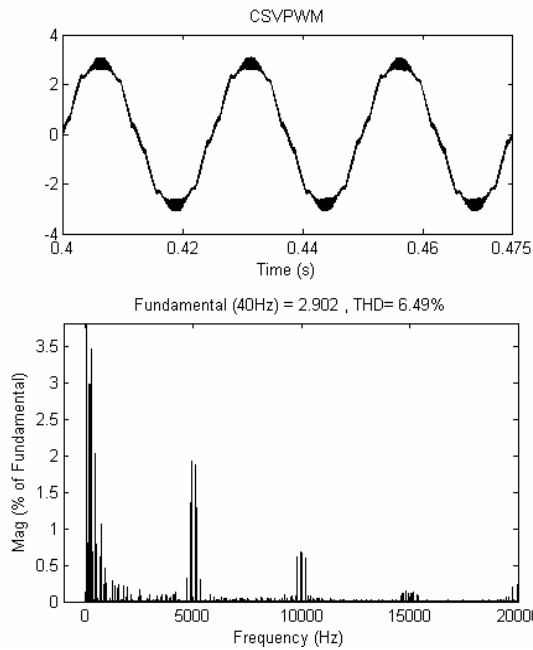


Figure-6a. Measured no-load current and harmonic spectra (% of fundamental) for CSVPWM at modulation index of 0.8.

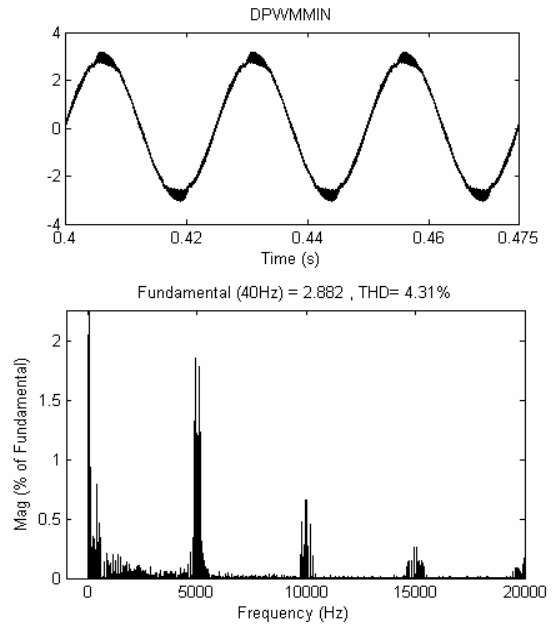


Figure-6c. Measured no-load current and harmonic spectra (% of fundamental) for DPWMMIN at modulation index of 0.8.

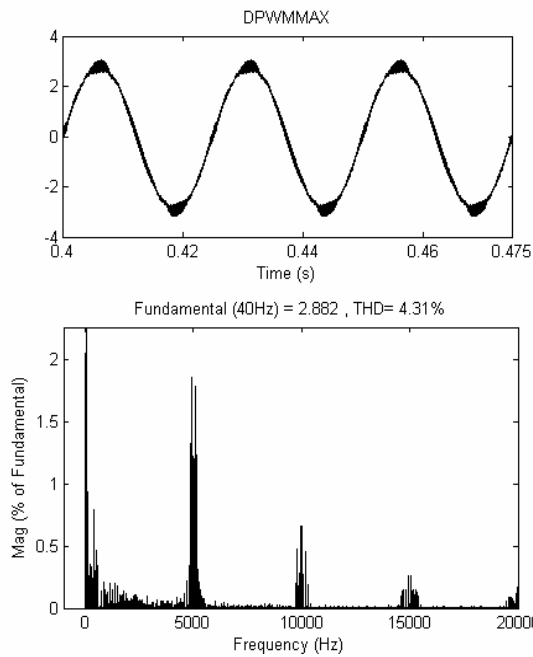


Figure-6b. Measured no-load current and harmonic spectra (% of fundamental) for DPWMMAX at modulation index of 0.8.

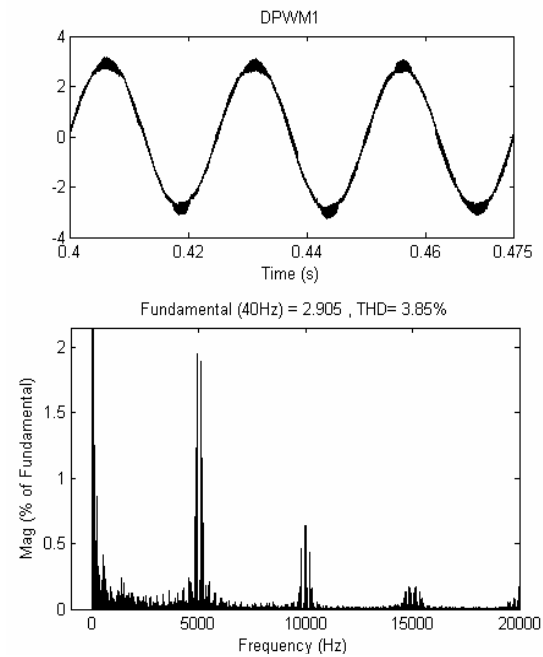


Figure-6d. Measured no-load current and harmonic spectra (% of fundamental) for DPWM1 at modulation index of 0.8.

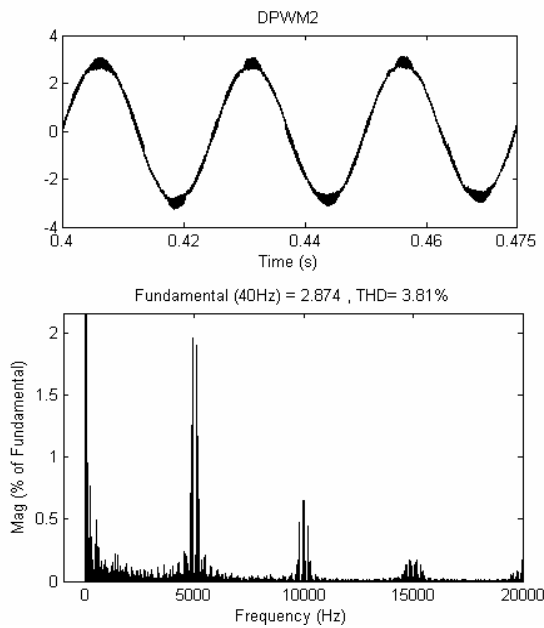


Figure-6e. Measured no-load current and harmonic spectra (% of fundamental) for DPWM2 at modulation index of 0.8.

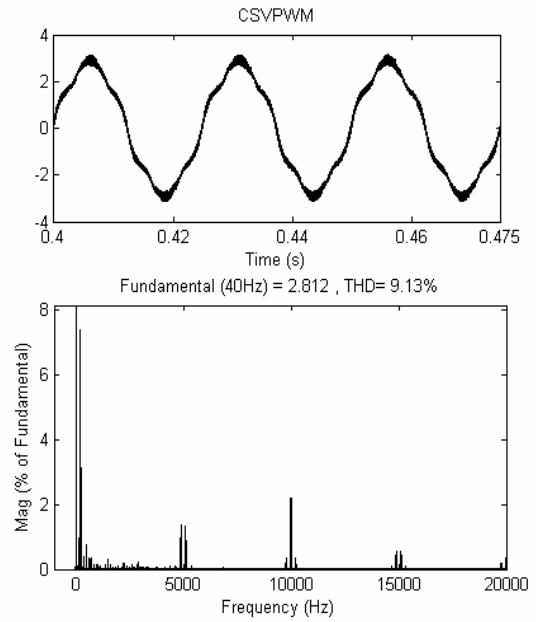


Figure-7a. Measured no-load current and harmonic spectra (% of fundamental) for CSVPWM at modulation index of 0.6.

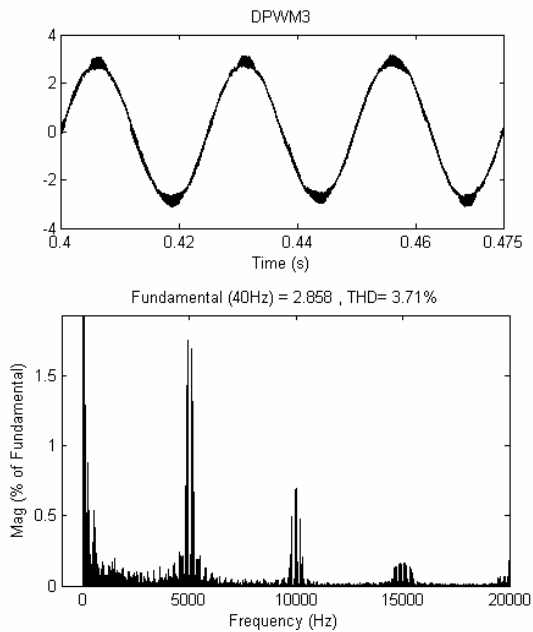


Figure-6f. Measured no-load current and harmonic spectra (% of fundamental) for DPWM3 at modulation index of 0.8.

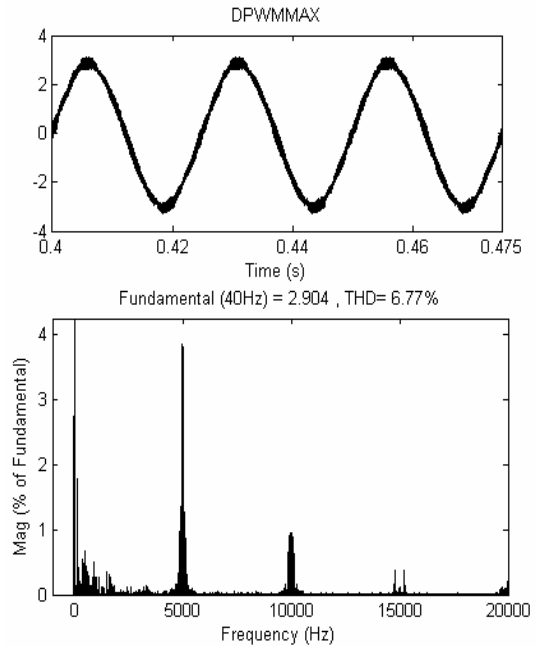


Figure-7b. Measured no-load current and harmonic spectra (% of fundamental) for DPWMMAX at modulation index of 0.6.

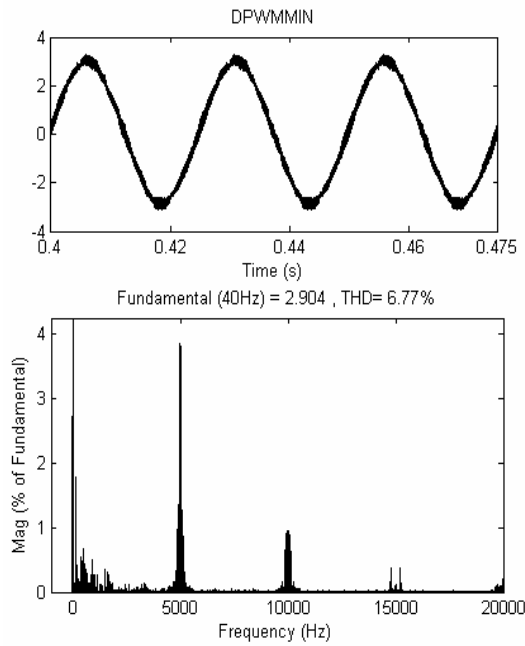


Figure-7c. Measured no-load current and harmonic spectra (% of fundamental) for DPWMMIN at modulation index of 0.6.

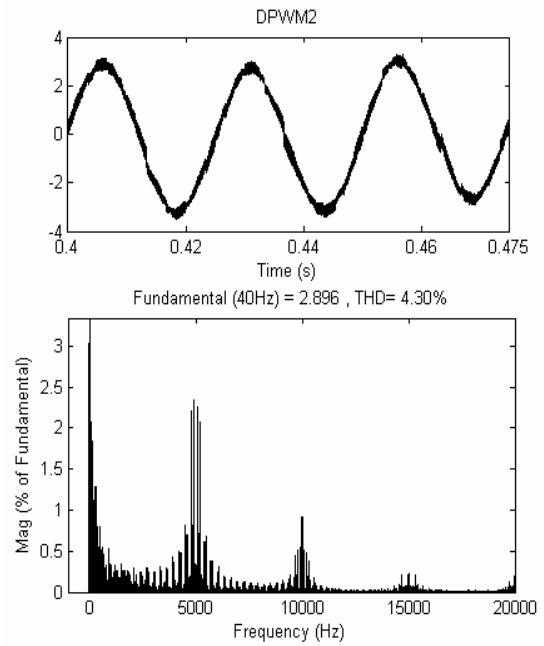


Figure-7e. Measured no-load current and harmonic spectra (% of fundamental) for DPWM2 at modulation index of 0.6.

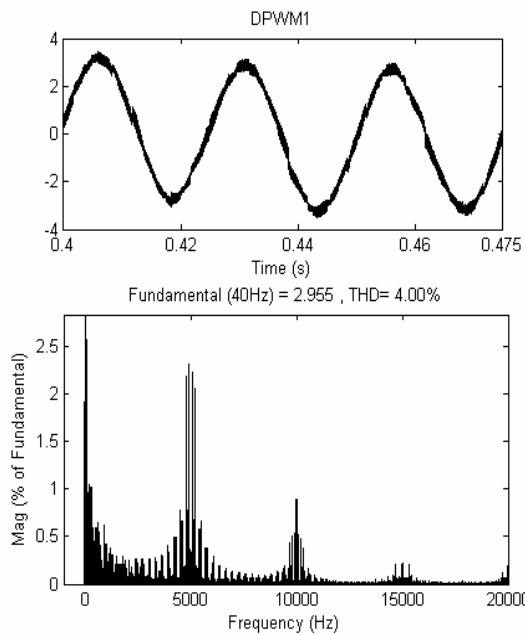


Figure-7d. Measured no-load current and harmonic spectra (% of fundamental) for DPWM1 at modulation index of 0.6.

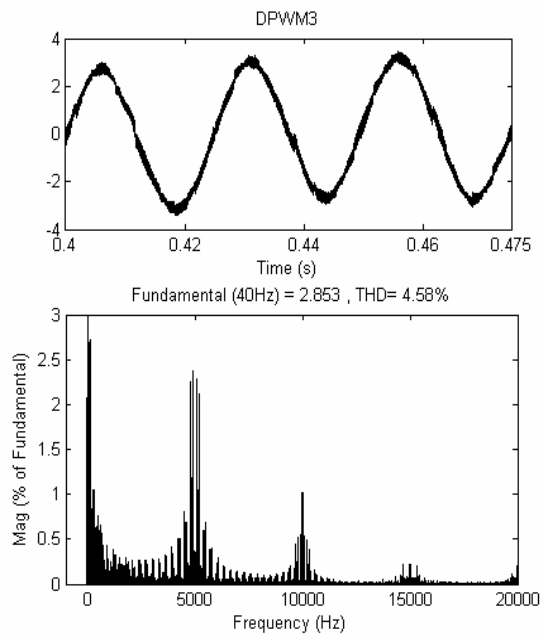


Figure-7f. Measured no-load current and harmonic spectra (% of fundamental) for DPWM3 at modulation index of 0.6.

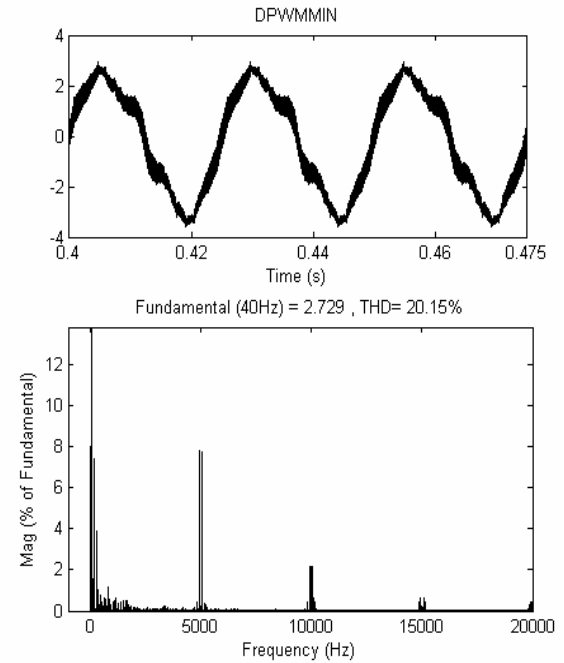
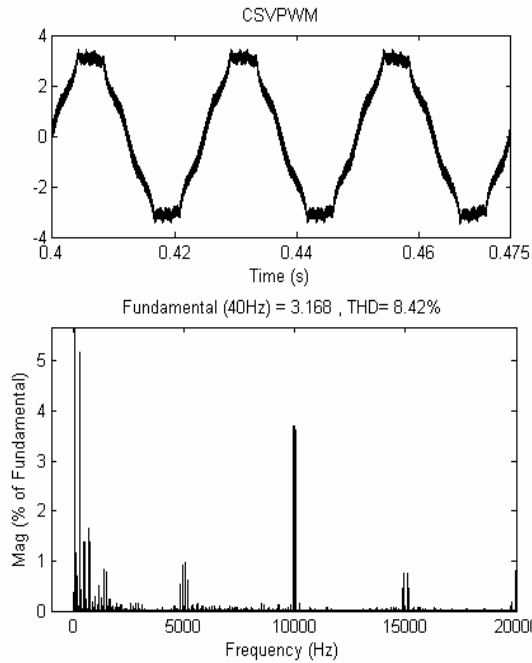


Figure-8a. Measured no-load current and harmonic spectra (% of fundamental) for CSVPWM at modulation index of 0.3.

Figure-8c. Measured no-load current and harmonic spectra (% of fundamental) for DPWMMIN at modulation index of 0.3.

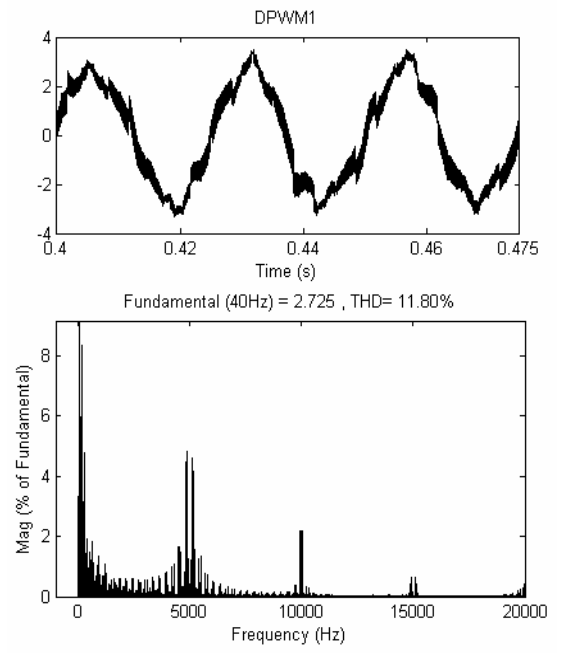
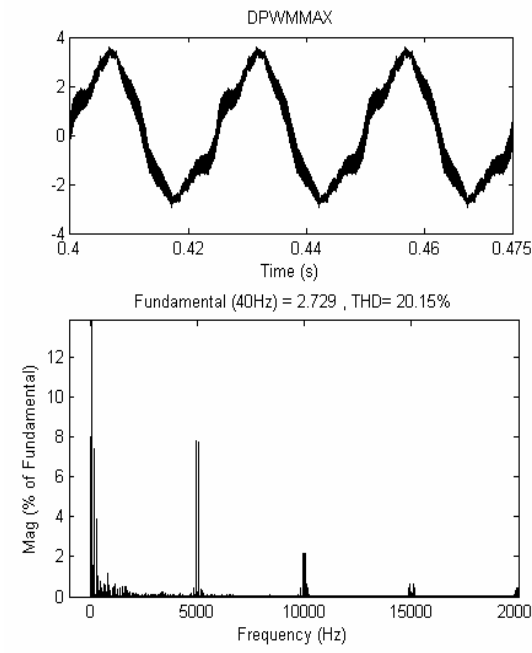


Figure-8b. Measured no-load current and harmonic spectra (% of fundamental) for DPWMMAX at modulation index of 0.3.

Figure-8d. Measured no-load current and harmonic spectra (% of fundamental) for DPWM1 at modulation index of 0.3.

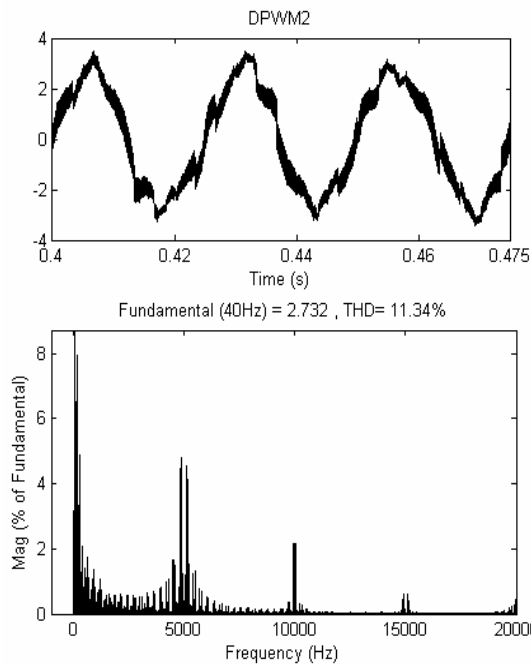


Figure-8e. Measured no-load current and harmonic spectra (% of fundamental) for DPWM1 at modulation index of 0.3.

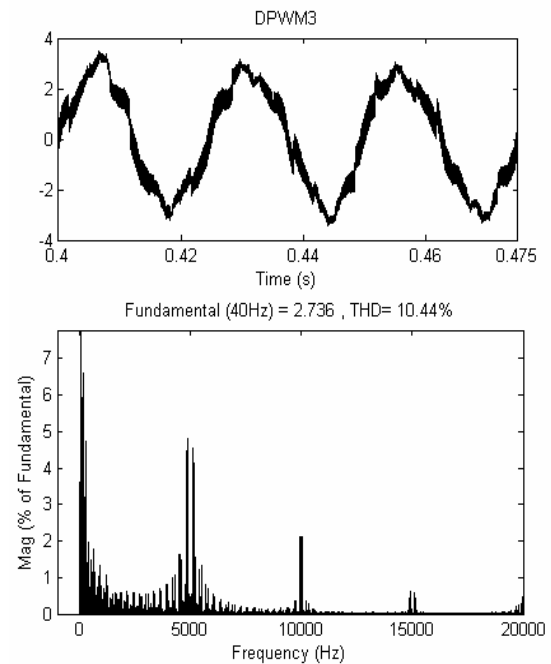


Figure-8f. Measured no-load current and harmonic Spectra (% of fundamental) for DPWM2 at modulation index of 0.3.

Table.1. Comparison of % THDs of various PWM methods at different modulation indices (M) and supply frequencies.

	M = 0.8		M = 0.6		M = 0.3	
	at 40Hz	at 50Hz	at 40Hz	at 50Hz	at 40Hz	at 50Hz
CSVPWM	6.49	7.2	9.13	9.99	8.42	9.38
DPWMMAX	4.31	5.26	6.77	8.11	20.15	21.47
DPWMMIN	4.31	5.20	6.77	8.10	20.15	22.61
DPWM1	3.85	5.45	4.00	11.23	11.80	21.97
DPWM2	3.81	5.41	4.30	9.54	11.34	19.65
DPWM3	3.71	5.04	4.58	9.48	10.44	19.79

From the simulation results it is once again proved that the better performance can be obtained by using CSVPWM at lower modulation indices and DPWM methods at higher modulation indices. Also computational burden involved in SV approach is eliminated with the utilization of imaginary switching times.

CONCLUSIONS

Among the popular PWM techniques CSVPWM has occupied renowned position because of its numerous advantages as stated earlier. To overcome the limitation i.e. poor performance at high modulation regions and computational burden involved, a simple and powerful novel space vector based generalized discontinuous PWM (GDPWM) algorithm with superior high modulation operating range performance characteristics and reduced

computational burden has been developed. This algorithm is utilized to illustrate and compare the performance characteristics of various PWM methods. The waveform quality comparisons in terms of %THDs indicate that CSVPWM at low-modulation and DPWM methods at the high-modulation range have superior performance. Also the execution time and memory required is reduced by eliminating the angle and sector estimation.

REFERENCES

- [1] J. Holtz. 1992. Pulse width modulation-A Survey. IEEE Trans. Ind. Electron. 39(5): 410-420.
- [2] J. Holtz. 1994. Pulse width modulation for electronic power conversion. Proc. IEEE. 82(8): 1194-1214.



- [3] Ahmet M. Hava, Russel J. Kerkman and Thomas A. Lipo. 1999. Simple Analytical and Graphical Methods for Carrier-Based PWM-VSI Drives. IEEE Trans. Power Electronics. 4(1): 49-61.
- [4] Ahmet M. Hava, Russel J. Kerkman and Thomas A. Lipo. 1998. A High Performance Generalized Discontinuous PWM Algorithm. IEEE Trans Ind appl. 34(5): 1059-1071.
- [5] Olorunfemi Ojo. 2004. The generalized discontinuous PWM scheme for three-phase voltage source inverters. IEEE Trans. Ind. Electron. 51(6): 1280-1289.
- [6] T. Brahmananda Reddy, J. Amarnath, D. Subba Rayudu and Md. Haseeb Khan. 2006. Generalized Discontinuous PWM Based Direct Torque Controlled Induction Motor Drive with a Sliding Mode Speed Controller. IEEE Proc. Power Electronics, Drives and Energy systems for Industrial Growth. PEDES'06, New Delhi, India, Paper No. 3D-11.
- [7] Keliang Zhou and Danwei Wang. 2002. Relationship between Space Vector Modulation and Carrier-Based PWM: A Comprehensive analysis. IEEE Trans. Ind. Electron. 49(1): 186-196.
- [8] G. Narayanan and V. T. Ranganathan. 2000. Triangle comparison and space vector approaches to Pulse width modulation in inverter-fed drives. J. Indian Inst. Sci. Vol. 80, pp. 409-427.
- [9] Joohn-Sheok Kim and Seung-Ki Sul. 1995. A novel voltage modulation technique of the space vector PWM. In: Proc. IPEC, Yokohama, Japan. pp. 742-747.
- [10] Dae-Woong Chung, Joohn-Sheok Kim and Seung-Ki Sul. 1998. Unified voltage modulation technique for real-time three-phase power conversion. IEEE Trans. Ind. Applicat. 34(2): 374-380.
- [11] Arbind Kumar. 2004. Direct Torque Control of Induction Motor is using imaginary switching Times with 0-1-2-7 AND 0-1-2 Switching Sequences: A Comparative Study. The 30th Annual Conference of the IEEE, IES. pp. 1492-1497.
- [12] T. Brahmananda Reddy, J. Amarnath and D. Subba Rayudu. 2006. New Hybrid SVPWM Methods for Direct Torque Controlled Induction Motor Drive for Reduced Current Ripple. IEEE Proc. Power Electronics, Drives and Energy systems for Industrial Growth, PEDES'06, New Delhi, India. Paper No.3B-20.